AIAA'83

AIAA-83-0532

Experimental Verification of Contact Conductance Models Based Upon Distributed Surface Micro-Hardness

M.M. Yovanovich and A. Hegazy, Univ. of Waterloo, Ontario, Canada; and V.W. Antonetti, International Business Machines Corp., Poughkeepsie, NY

AIAA 21st Aerospace Sciences Meeting

January 10-13, 1983/Reno, Nevada

EXPERIMENTAL VERIFICATION OF CONTACT CONDUCTANCE MODELS BASED UPON DISTRIBUTED SURFACE MICRO-HARDNESS

M.M. Yovanovich*, A. Hegazy** and V.W. Antonetti†
Thermal Engineering Group
Department of Mechanical Engineering
University of Waterloo
Waterloo, Ontario, N2L 3G1

Abstract

Previously published contact conductance models: BHM (Bulk Hardness), ITM (Iterated), INM (Integral) and DAM (Direct Approximate) are compared with data for Ni 200 specimens having surface parameters (σ=1.21 to 8.48 μm; m = .139 to .344) and micro-hardness ranging from 170 to 362 kg/mm^2. Contact pressure varied from 518 to 3636 kN/m^2. Experimental results demonstrate the inadequacy of the BHM in general for predicting contact conductances. BHM predictions exceeded measurements by 65 to 94%. ITM predictions are in good agreement, while the INM and DAM predictions are in excellent agreement with all data. Effective micro-hardness varied from 277 to 362 kg/mm^2. The study clearly shows the importance of the micro-hardness layer and the adequacy of the new models.

Nomenclature

$\bar{a}$	=	mean contact spot radius
BH	=	Brinell hardness number
BHM	=	bulk hardness model
c_1, c_2, c_3	=	correlation constants
C_c	=	$\sigma h_c / k_s$, dimensionless contact conductance
DAM	=	direct approximate hardness model
H	=	hardness
H_b, H_e, H_{mn}, H_{mx}	=	bulk, effective, minimum and maximum hardness
h_c	=	contact conductance
INM	=	integral hardness model
ITM	=	iterated hardness model
k_1, k_2	=	conductivities of contacting asperities
k_s	=	harmonic mean conductivity
m_1, m_2	=	mean absolute surface slope of contacting surfaces
m	=	$\sqrt{m_1^2 + m_2^2}$ effective absolute surface slope
$P, \bar{P}, P_{mn}, P_{mx}$	=	contact, mean, minimum and maximum pressures
RH	=	Rockwell hardness number
T, ΔT_c	=	temperature and contact temperature drop
T_{e1}, T_{e2}	=	extrapolated surface temperatures
t, $\bar{t}$	=	penetration and mean penetration depth
t_o, t_b	=	penetration at maximum and bulk hardness
Y	=	separation of mean planes of surfaces

Greek Symbols

β	=	dummy variable
ξ	=	ITM parameter
σ_1, σ_2	=	RMS surface roughness of contacting surfaces
σ	=	$\sqrt{\sigma_1^2 + \sigma_2^2}$ effective surface roughness

Introduction

Thermal contact conductance models incorporating surface micro-hardness distributions were presented recently by Yovanovich, Hegazy and De Vaal[1]. It was shown that the conventional mechanical model which assumes uniform hardness equal to the bulk value (BHM) gives an upper bound on contact conductances. On the other hand the integrated hardness model (INM) gives a lower bound on contact conductances, and the direct approximate model (DAM) predicts contact conductances nearly equal to those of the INM. The iterated hardness model (ITM) predicts contact conductances between the upper and lower bounds.

The predictions of contact conductances by the different hardness models were compared with limited experimental data.[1] It was observed that the predictions of the BHM and the measured values differed by approximately 58 to 85 percent. The INM and DAM predictions were observed to be in excellent agreement with the limited data, and those of the ITM were in good agreement with the data.

It is the purpose of this paper to describe an experimental program conducted to obtain additional contact conductance data for several specimens possessing different surface characteristics and the same surface micro-hardness distribution, and further to compare the measured contact conductances against the theoretical values based upon the different hardness models.

Review of Contact Conductance Models

The four contact conductance models are denoted as BHM (bulk hardness), ITM (iterated), INM (integral) and DAM (direct approximate) models.

The BHM assumes isotropic hardness throughout the surface asperities equal to the bulk value corresponding to either Rockwell or Brinell hardness tests.

The ITM is based upon the surface micro-hardness distribution and a scheme for locating the surface asperities within the micro-hardness layer. The parameter ξ is employed to set the surface asperities within the layer at zero contact pressure. An iterative program is then used to compute the effective surface hardness for the particular surface and contact pressure. The effective hardness decreases with increasing contact pressure corresponding to the penetration depth.

In the INM it is assumed that each asperity has a hardness distribution corresponding to the hardness layer. By means of an integral it is possible to compute an effective hardness corresponding to a particular surface and the applied

* Professor, Associate Fellow AIAA
** Graduate Research Assistant
† Senior Engineer, IBM Corp., Poughkeepsie, N.Y.

load. The following expressions permit computation of the effective hardness.

$$\frac{He}{H_{mx}} = \frac{Num}{Den} \quad (1)$$

where

$$Num = \int_{Y/\sigma}^{\infty} (\beta - Y/\sigma) H^*(\beta - Y/\sigma) \exp[-0.5(\beta - 0.7)^2] d\beta \quad (2)$$

and

$$Den = \int_{Y/\sigma}^{\infty} (\beta - Y/\sigma) \exp[-0.5(\beta - 0.7)^2] d\beta \quad (3)$$

The normalized hardness distribution can be written as

$$H^*(\beta - Y/\sigma) = 1, \quad (\beta - Y/\sigma) \leq t_o/\sigma$$

$$H^*(\beta - Y/\sigma) = c_1 \sigma^{c2} (\beta - Y/\sigma)^{c2} + C_3, \quad t_o/\sigma \leq (\beta - Y/\sigma) \leq t_b/\sigma \quad (4)$$

$$H^*(\beta - Y/\sigma) = H_b/H_{mx}, \quad (\beta - Y/\sigma) \geq t_b/\sigma$$

The constants, c_1, c_2 and c_3 which appear in Equation (4) are the correlation constants for the hardness layer given in Figure 1.

The normalized separation is determined by means of

$$Y/\sigma = 1.184 \, [\ell n \, (3.132 \, P/H_b)]^{0.547} \quad (5)$$

For all practical cases the upper limit in Equations (2) and (3) can be set equal to 3.

In the DAM the effective hardness is determined for a particular surface at the mean contact pressure. The effective hardness is then used for all contact pressures between the minimum and maximum contact pressures. The following procedure can be followed to determine the effective hardness.

The mean contact spot radius depends upon surface characteristics, mean contact pressure and the bulk hardness:

$$\bar{a} = 0.99(\sigma/m)/[-\ell n(3.132 \, \bar{P}/H_b)]^{0.547} \quad (6)$$

The mean penetration depth can be related to the mean contact spot radius:

$$\bar{t} = (\pi \bar{a}^2/24.5)^{1/2} = 0.358 \, \bar{a} \quad (7)$$

Upon substitution of the mean penetration depth into the micro-hardness correlation one obtains the effective hardness:

$$H_e = H(\bar{t}) = c_1 (0.358 \bar{a})^{c2} + c_3 \quad (8)$$

For the Nickel 200 specimens having the micro-hardness distribution shown in Figure 1 we find

$$H_e(kg/mm^2) = 11.38(m/\sigma)^{0.274} [-\ell n(3.132 \bar{P}/H_b)]^{0.150} + 7.79 \quad (9)$$

If the calculated value of H_e exceeds the maximum value measured, then use the maximum value. The computed effective hardness values are given in Table 1 for the reported surface characteristics and mean contact pressure.

Experimental Program and Test Results

Test Specimens

All test specimens were fabricated from a single Nickel 200 rod. The individual specimens were finished to 28.6 mm in diameter by 31.8 mm long, both ends being carefully lapped smooth and flat. The specimens were, of course, tested in pairs, with one of the pair treated further by glass bead blasting one end to a specified roughness.

The surface characteristics of the specimens as measured using a Rank-Taylor-Hobson Talysurf 5 profilometer are shown in Table 1. Contact surface flatness deviation was determined optically and in all cases was less than 1 micron.

Table 1 Geometric, thermophysical properties and pressure range of test specimens

Specimen	1	2	3	4	5	6	7	8
σ_i, μm	1.19	0.19	4.27	0.17	4.29	0.16	8.48	0.14
m_i	0.137	0.024	0.236	0.024	0.239	0.025	0.344	0.018
σ, μm	1.21		4.27		4.29		8.48	
m	0.139		0.237		0.240		0.344	
P_{mn}, kP_a	622		518		698		571	
P_{mx}, kP_a	3510		3215		3636		3433	
$\bar{P}$, kP_a	2066		1866.5		2167		2002	
H_e, kg/mm^2	362.3		302.0		301.5		277.3	
H_b, kg/mm^2	170.4		170.4		170.4		170.4	

Calibrated No. 30 gauge copper-constantan thermocouples were installed at four axial positions in each specimen. The thermocouples were placed into slightly oversized holes (0.5 mm diameter) drilled to a depth of 2.5 mm, and were secured with a silver epoxy (k = 2 W/mK). All thermocouple leads were wrapped once around the specimens to reduce heat loss from the wire.

Hardness measurements were made using Vickers, Rockwell and Brinell indenters. Figure 1 shows the measured values versus depth of penetration. The maximum value H_{mx} = 362.3 kg/mm^2 was observed at a penetration depth of 1.24 μm and the minimum or bulk value H_b = 170.4 kg/mm^2 was observed at penetration depths greater than t_b = 21.56 μm. The measured Vickers surface micro-hardness values were correlated by means of the following expression:

$$H(t) = c_1 t^{c2} + c_3 \quad (10)$$

where c_1 = 377.27, c_2 = -0.274 and c_3 = 7.79

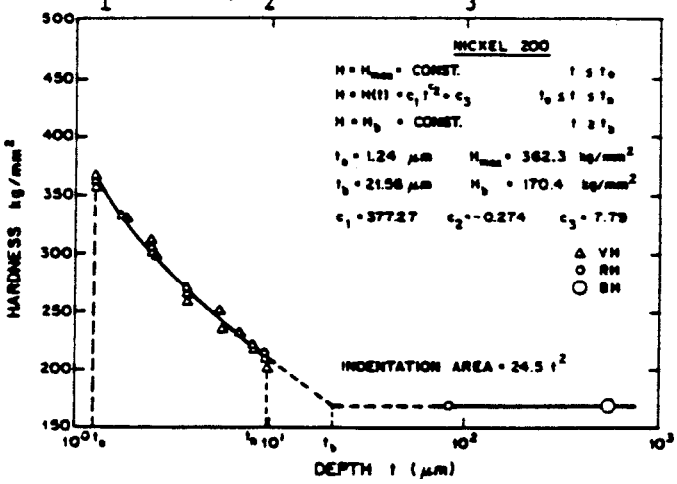

Fig. 1 Hardness distribution of Nickel 200

Test Apparatus

Contact resistance measurements were made in a vacuum chamber at an ambient pressure of approximately 10^{-4} mm Hg. A schematic of the test column with radiation shields removed is shown in Figure 2. Note the heat flow direction was always from the

upper test specimen, which had the bead-blasted rough surface, to the smooth surfaced lower specimen.

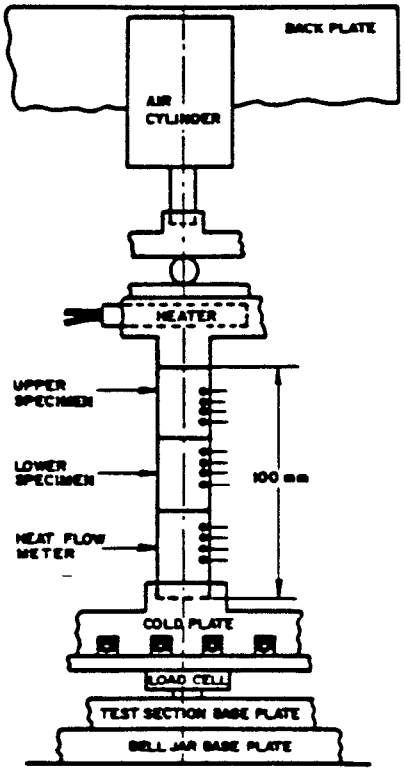

Fig. 2 Schematic sketch of test apparatus

The diaphragm-type air cylinder located within the vacuum chamber allowed an axial force to be applied by adjusting an external nitrogen pressure source. This technique has the advantage of not requiring that the vacuum be broken to effect a load change. Because a diaphragm-type air cylinder is, in a practical sense, frictionless, and because a large reservoir was used in the line between the air cylinder and the nitrogen pressure regulating valve, thermal expansion of the test column was accommodated without any noticeable change in the measured axial load. The apparent contact pressure was determined from the output of a Sensotec model 53 strain-gauge type load cell. Uniform loading of the specimens was assured by applying the force to the test column through a 13 mm steel ball located in the upper portion of the column and also by having a load cell with a hemispherical bullet mount on the opposite end of the column.

The heat source was a Watlow stainless steel cartridge-type 200 watt heater which was silver epoxied into a cylindrical copper block. Since copper tarnishes so readily, a thin layer of gold was vapor-deposited on the copper block at the critical section where the copper would contact the upper test specimen. The heat sink was a copper cold plate cooled by a closed-loop water chiller system. The heat load was measured at two locations: First, the input electrical power to the test specimens was found by monitoring the voltage drop across the heater and computing the current from the voltage drop across a precision resistor in series with the heater. Second, the heat flow existing the test section was determined by positioning below the lower test specimen an ARMCO Iron cylinder of known thermal conductivity, measuring the temperature gradient in the ARMCO Iron and calculating the heat flow rate using Fourier's equation.

The thermal conductivity of the Nickel 200 test specimens was found experimentally by running the test apparatus with a single specimen, measuring the temperature gradient, and requiring that the difference between the input electrical power and the exiting ARMCO power be less than 5 percent. Over the temperature range of interest the thermal conductivity was determined to be

$$k = 73.1 - 0.0553\ T \qquad (11)$$

where T is the temperature of the Nickel 200 in degrees Celsius. The thermal conductivity values given by Eq. (11) are in good agreement with published data.

Test Procedure

Under the control of an IBM 5100 computer, a Fluke Datalogger scanned and read the thermocouples, the load cell output voltage and the heater voltages. Test specimen temperature gradients were extrapolated to the test interface by a first order least squares polynomial approximation.

Three criteria were used to establish thermal equilibrium:

1) A maximum difference of 7.5 percent between the electrical input power and the heat flow rate determined from the ARMCO.
2) A maximum difference of 3.0 percent between an interface resistance value and a prior value calculated 3 minutes earlier.
3) A maximum difference of 0.1°C between a lower test specimen thermocouple reading and a prior reading taken 3 minutes earlier.

Once steady state was achieved, the data were read, reduced and stored on tape. A summary of pertinent experimental results is presented in Tables 2 through 5 for the test specimens described in Table 1.

Table 2 Test results for specimens 1 and 2

P kPa	ΔT_c °C	T_m °C	k_1 W/mK	k_2 W/mK	h_c kW/m^{2}K	$10^5 C_c$
662	35.3	150	63.8	65.8	2.658	4.96
980	22.4	141	64.7	65.9	4.182	7.75
1624	14.6	134	65.3	66.1	6.500	11.97
2105	10.7	132	65.5	66.1	8.814	16.21
2837	13.3	188	62.3	63.1	10.759	20.76
3510	10.9	185	62.6	63.2	13.110	25.23

Table 3 Test results for specimens 3 and 4

P kPa	ΔT_c °C	T_m °C	k_1 W/mK	k_2 W/mK	h_c kW/m^{2}K	$10^5 C_c$
518	44.2	107	66.0	68.4	1.247	7.93
[illegible]50	21.7	99.5	67.2	68.4	2.533	15.96
1457	16.4	91.3	67.6	68.5	3.312	20.80
1827	13.0	89.3	67.8	68.5	4.095	25.67
2150	12.4	88.7	67.9	68.5	4.322	27.08
3215	10.5	111.0	66.7	67.3	7.359	46.96

Table 4 Test results for specimens 5 and 6

P kPa	ΔT_c °C	T_m °C	k_1 W/mK	k_2 W/mK	h_c kW/m^{2}K	$10^5 C_c$
698	35.1	114	65.8	67.8	1.749	11.24
1194	23.3	107	66.5	67.8	2.747	17.55
1559	16.2	98.8	67.2	68.1	3.950	25.07
1925	14.3	99.8	67.2	68.0	4.358	27.68
2450	12.2	97.4	67.4	68.1	5.183	32.86
2890	11.8	118	66.3	66.9	6.583	42.45
3636	9.0	116	66.4	66.9	8.619	55.49

Table 5 Test results for specimens 7 and 8

P [illegible]a	ΔT_c °C	T_m °C	k_1 W/mK	k_2 W/mK	h_c kW/m^{2}K	$10^5 C_c$
[illegible]571	49.7	107	65.8	68.6	1.013	12.79
976	30.6	95.1	67.0	68.7	1.681	21.02
1591	17.2	87.3	67.8	68.8	2.938	36.50
2080	13.9	85.1	68.0	68.8	3.697	45.84
2719	20.5	138.6	64.9	66.0	4.815	62.41
3433	17.6	136.5	65.1	66.0	5.632	72.87

The data reported in Tables 2 to 5 are the nominal contact pressure, temperature drop across the interface, mean interface temperature, thermal conductivities of the contacting asperities, contact conductance and the dimensionless contact conductance.

The extrapolated temperature T_{e1}, T_{e2}, the mean interface temperature T_m and the temperature drop ΔT_c are related by the following expressions:

$$T_{e1} = T_m + \Delta T_c/2 \qquad (12)$$

$$T_{e2} = T_m - \Delta T_c/2$$

The thermal conductivities reported in Tables 2 to 5 are computed by means of Eq. (11) for the temperature levels determined by means of Eq. (12).

Comparison of Theory and Experimental Results

Experimental and theoretical dimensionless [illegible]tact conductances versus contact pressure are presented in Figures 3 through 10. The theoretical values predicted by the BHM, ITM and INM models are shown in Figures 3 through 6 and the DAM values are shown in Figures 7 through 10. Also experimental, BHM and DAM dimensionless contact conductances are presented in Tables 6 through 9.

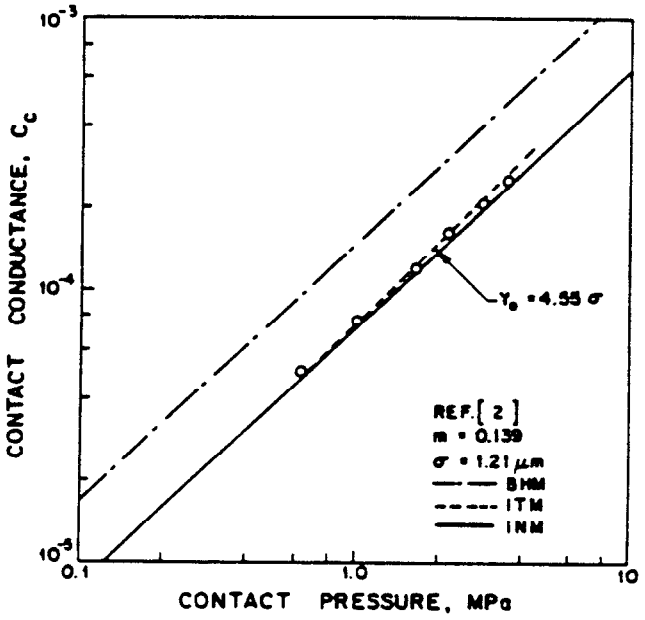

Figure 3. Comparison between the BHM, ITM, INM and the experiments for specimens 1 and 2.

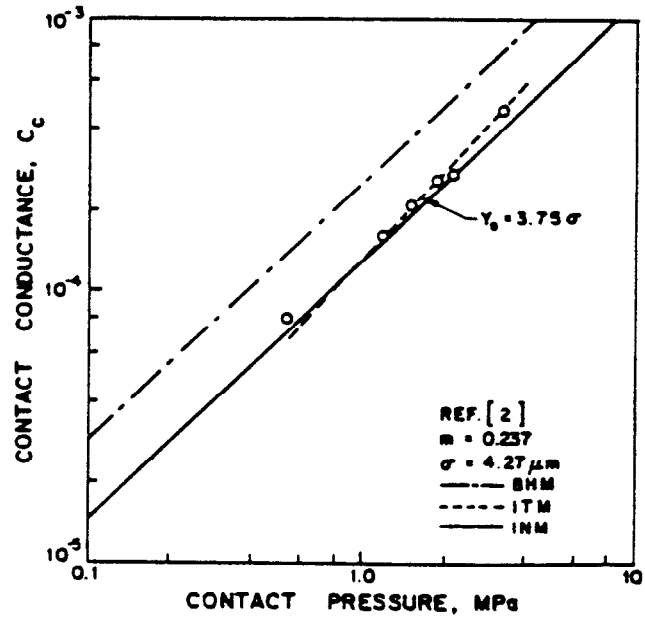

Fig. 4. Comparison between the BHM, ITM, INM and the experiments for specimens 3 and 4.

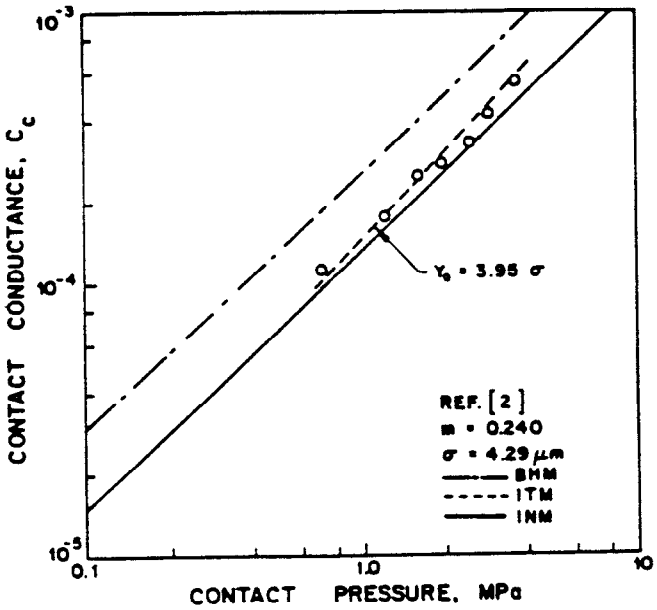

Fig. 5. Comparison between the BHM, ITM, INM and the experiments for specimens 5 and 6.

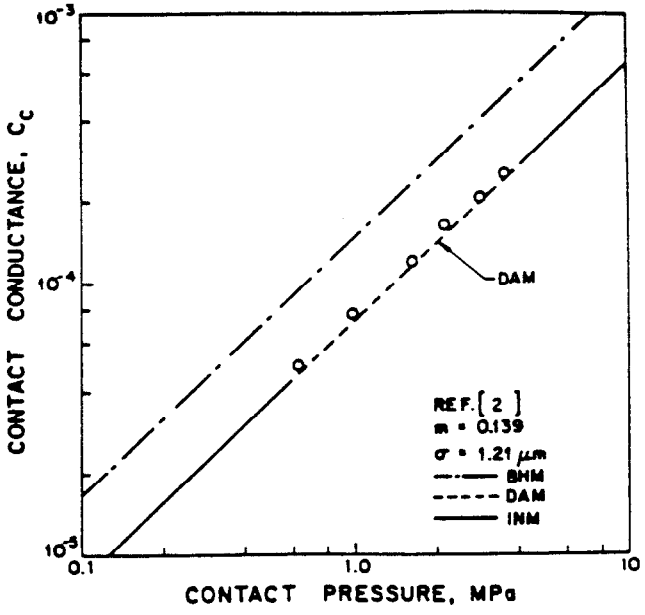

Fig. 7 Comparison between the BHM, DAM, INM and the experiments for specimens 1 and 2

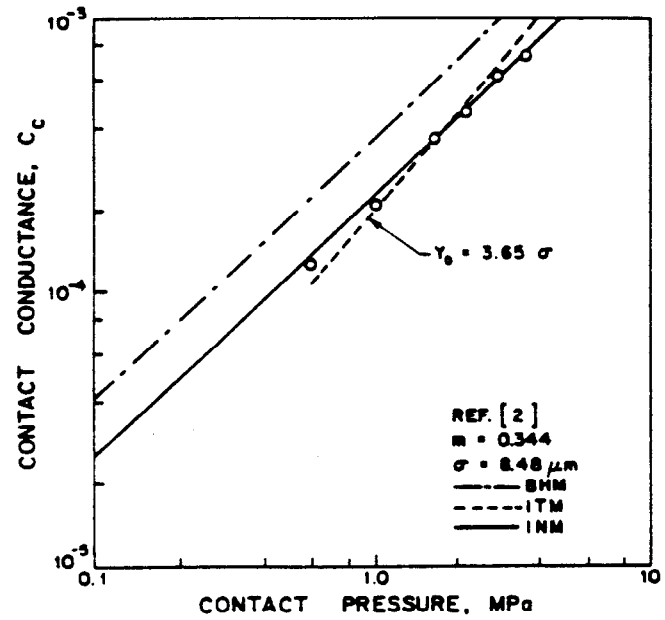

Fig. 6 Comparisons between the BHM, ITM, INM and the experiments for specimens 7 and 8.

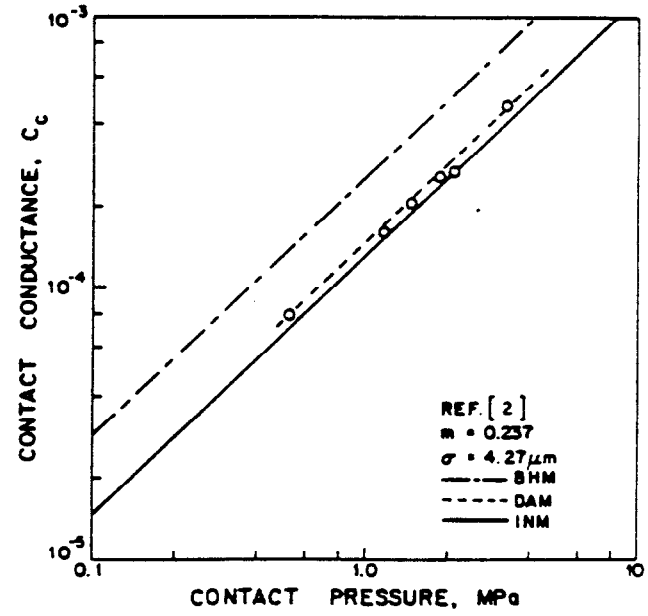

Fig. 8 Comparisons between the BHM, DAM, INM and the experiments for specimens 3 and 4

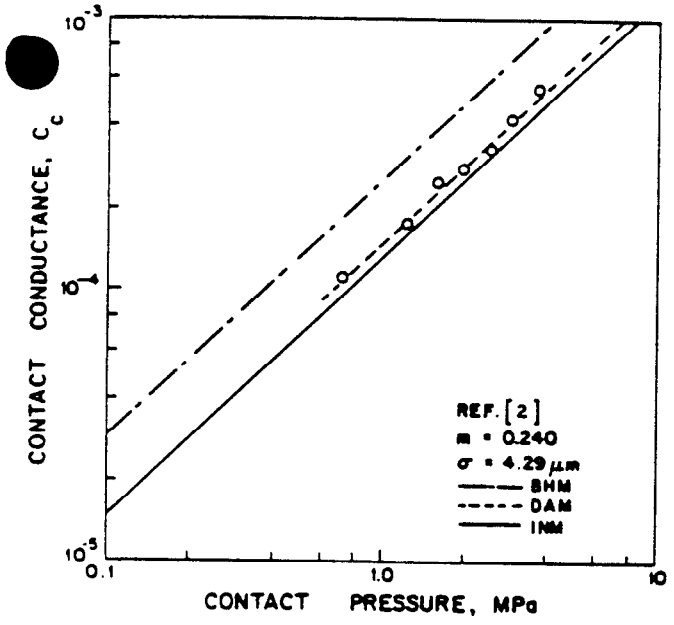

Fig. 9 Comparison between the BHM, DAM, INM and the experiments for specimens 5 and 6

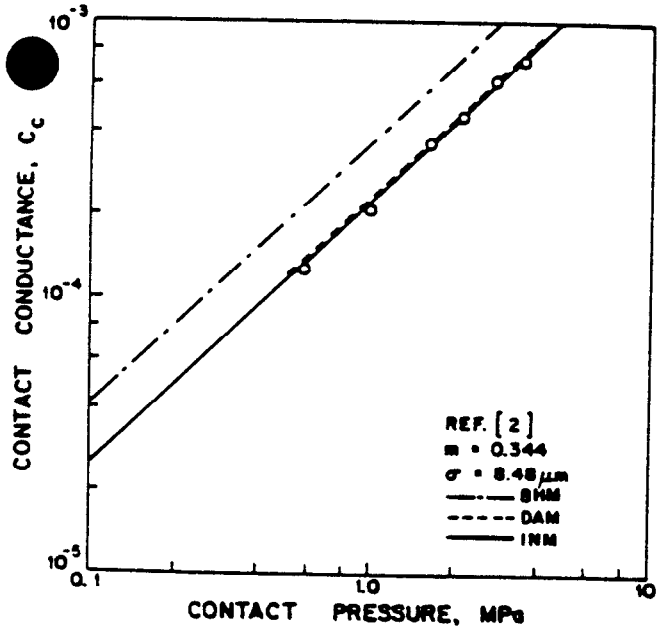

Fig. 10 Comparison between the BHM, DAM, INM and the experiments for specimens 7 and 8

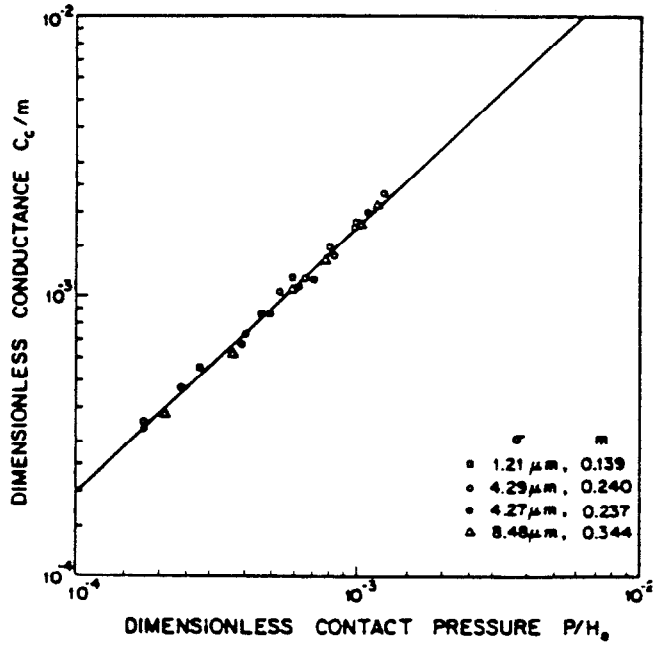

Fig. 11 Comparison between the DAM and the experiments for all the specimens.

From Figures 3 through 6 it can be seen that there is good agreement between the ITM values and the data. From Figures 7 through 10 it can be seen that the DAM and INM values are nearly equal and in excellent agreement with the data for all specimens and all contact pressures. The excellent agreement between the DAM values and the data can also be seen in Tables 6 through 9 where the RMS percent difference is approximately 5-6 for all specimens.

Figures 3 through 6 and the tabulated values given in Tables 6 through 9 show the very poor agreement between the BHM values and the data. The error ranges from approximately 65% for the roughest surface up to approximately 94% for the smoothest surface.

To demonstrate further the excellent agreement between the DAM predictions and the data, the dimensionless contact conductance divided by the effective absolute surface slope, C_c/m, is plotted against dimensionless contact pressure, P/He, for all specimens in Figure 11. The theoretical curve based upon the DAM model is seen to be an excellent correlation of all data points.

Conclusions and Recommendation

The experimental results demonstrate clearly the importance of the micro-hardness layer produced within Nickel 200 by lapping. The conventional contact conductance model based upon the bulk hardness (BHM) is totally inadequate in predicting contact conductances. The ITM can be used to predict contact conductances which will be in good to adequate agreement with data. The INM and DAM contact conductance values are very nearly equal for all specimens and in excellent agreement with all data.

It is therefore recommended that the simple

Table 6 Comparison between test results, BHM and DAM models for specimens 1 and 2

P kPa	$10^4 C_c$ test	$10^4 C_c$ BHM	$10^4 C_c$ DAM	% Diff BHM	%Diff. DAM
622	0.496	0.959	0.469	93.35	-5.44
980	0.775	1.478	0.722	90.71	-8.84
1624	1.197	2.388	1.166	99.50	-2.59
2105	1.621	3.055	1.492	88.46	-7.96
2837	2.076	4.057	1.981	95.42	-4.58
3510	2.523	4.966	2.425	96.83	-3.88
		RMS % Difference		94.12	-5.97

Table 7 Comparison between test results, BHM and DAM models for specimens 3 and 4

P kPa	$10^4 C_c$ test	$10^4 C_c$ BHM	$10^4 C_c$ DAM	% Diff. BHM	%Diff. DAM
518	0.793	1.375	0.798	73.39	0.63
1150	1.596	2.933	1.703	83.77	6.70
1457	2.080	3.672	2.132	76.54	2.50
1827	2.567	4.553	2.644	77.37	3.00
2150	2.708	5.148	2.989	90.10	10.38
3215	4.696	7.789	4.522	65.86	-3.71
		RMS % Difference		78.21	5.51

Table 8 Comparison between test results, BHM and DAM models for specimens 5 and 6

P kPa	$10^4 C_c$ test	$10^4 C_c$ BHM	$10^4 C_c$ DAM	% Diff. BHM	% Diff. DAM
698	1.124	1.848	1.075	64.41	-4.36
1194	1.755	3.078	1.790	75.38	1.99
1559	2.507	3.966	2.306	58.20	-8.02
1925	2.768	4.846	2.819	75.07	1.84
2450	3.286	6.093	3.544	85.42	7.85
2890	4.245	7.128	4.146	67.92	-2.33
3636	5.549	8.866	5.156	59.78	-7.08
		RMS % Difference		70.04	5.44

Table 9 Comparison between test results, BHM and DAM models for specimens 7 and 8

P kPa	$10^4 C_c$ test	$10^4 C_c$ BHM	$10^4 C_c$ DAM	%Diff. BHM	%Diff. DAM
571	1.279	2.189	1.378	71.15	7.74
976	2.102	3.643	2.293	73.31	9.087
1591	3.650	5.795	3.648	58.77	-0.05
2080	4.584	7.476	4.706	63.09	2.66
2719	6.241	9.642	6.070	54.49	-2.74
3433	7.287	12.033	7.575	65.13	3.95
		RMS % Difference		64.65	5.36

direct approximate model (DAM) should be used to predict contact conductances for conforming rough surfaces.

Acknowledgements

The authors (M.M.Y., A.H.) acknowledge the financial support of AECL Whiteshell Nuclear Reactor Establishment under contract File A-7662 and the partial support of the National Science and Engineering Research Council of Canada under operating grant A-7445.

The authors also thank Dr. M.H. Schankula and Mr. J. DeVaal for their assistance and advice.

References

1. Yovanovich, M.M., Hegazy, A. and DeVaal, J., "Surface Hardness Distribution Effects Upon Contact, Gap and Joint Conductances", AIAA Paper No. 82-0887, AIAA/ASME 3rd Joint Thermophysics, Fluids, Plasma and Heat Transfer Conference, June 7-11, 1982, St. Louis, Missouri.

2. Antonetti, V.W., Ph.D. Thesis in progress, Department of Mechanical Engineering, University of Waterloo.